

## Giant Isotope Effect of Thermal Conductivity in Silicon Nanowires

Penghong Ci<sup>1,2,3</sup>, Muhua Sun<sup>4</sup>, Meenakshi Upadhyaya<sup>5</sup>, Houfu Song<sup>6</sup>, Lei Jin<sup>1</sup>, Bo Sun<sup>6,7</sup>,  
Matthew R. Jones<sup>4</sup>, Joel W. Ager<sup>1,2</sup>, Zlatan Aksamija<sup>5,\*</sup> and Junqiao Wu<sup>1,2,†</sup>

<sup>1</sup>*Department of Materials Science and Engineering, University of California, Berkeley, California 94720, USA*

<sup>2</sup>*Materials Sciences Division, Lawrence Berkeley National Laboratory, Berkeley, California 94720, USA*

<sup>3</sup>*Institute for Advanced Study, Shenzhen University, Shenzhen 518060, China*

<sup>4</sup>*Department of Chemistry, Rice University, Houston, Texas 77005, USA*

<sup>5</sup>*Department of Electrical and Computer Engineering, University of Massachusetts-Amherst, Amherst, Massachusetts 01003, USA*

<sup>6</sup>*Tsinghua-Berkeley Shenzhen Institute (TBSI), Tsinghua University, Shenzhen 518055, China*

<sup>7</sup>*Tsinghua Shenzhen International Graduate School and Guangdong Provincial Key Laboratory of Thermal Management Engineering and Materials, Shenzhen 518055, China*

 (Received 3 June 2021; revised 11 November 2021; accepted 31 January 2022; published 23 February 2022)

Isotopically purified semiconductors potentially dissipate heat better than their natural, isotopically mixed counterparts as they have higher thermal conductivity ( $\kappa$ ). But the benefit is low for Si at room temperature, amounting to only  $\sim 10\%$  higher  $\kappa$  for bulk  $^{28}\text{Si}$  than for bulk natural Si ( $^{\text{nat}}\text{Si}$ ). We show that in stark contrast to this bulk behavior,  $^{28}\text{Si}$  (99.92% enriched) nanowires have up to 150% higher  $\kappa$  than  $^{\text{nat}}\text{Si}$  nanowires with similar diameters and surface morphology. Using a first-principles phonon dispersion model, this giant isotope effect is attributed to a mutual enhancement of isotope scattering and surface scattering of phonons in  $^{\text{nat}}\text{Si}$  nanowires, correlated via transmission of phonons to the native amorphous  $\text{SiO}_2$  shell. The Letter discovers the strongest isotope effect of  $\kappa$  at room temperature among all materials reported to date and inspires potential applications of isotopically enriched semiconductors in microelectronics.

DOI: [10.1103/PhysRevLett.128.085901](https://doi.org/10.1103/PhysRevLett.128.085901)

Thermal management is one of the major bottlenecks to continued scaling of modern microelectronics beyond the current generation, as devices in integrated circuits become increasingly smaller, denser, and more power hungry [1,2]. It is desired to have the active channel of these micro-devices made of semiconductors that not only perform the electronic functions needed, but also quickly dissipate heat away. For silicon, this requirement presents a critical challenge. Although bulk, crystalline Si has a relatively high thermal conductivity ( $\kappa \sim 144$  W/mK at room temperature), when its size is reduced to the submicron range,  $\kappa$  is strongly suppressed owing to significant boundary scattering of phonons [3,4]. The reduction in  $\kappa$  becomes even more severe when the surface of the size-reduced Si is rough [5–7], noting that surface or interface roughness exists ubiquitously to a certain degree, especially in nano-structures fabricated via top-down approaches involving chemical etching. It has been reported that, for example, for Si nanowires (NWs) with surface roughness of  $\sim 3$  nm,  $\kappa$  is reduced to the level of  $\sim 5$  W/mK when the diameter is below 100 nm [5,6]. This  $\kappa$  suppression becomes a critical problem for heat dissipation in field effect transistors (FETs) lithographically fabricated from Si wafers, such as fin field effect transistors (FinFETs), [8] and gate-all-around FETs [9]. Alternative materials with high  $\kappa$  near room temperature have been recently investigated as heat dissipation materials for microelectronics, such as boron

phosphide (BP,  $\sim 490$  W/mK) [10], cubic boron nitride (cBN,  $\sim 880$  W/mK) [11], and boron arsenide (BAs,  $\sim 1000$  W/mK) [11–13]. Yet it would be much more impactful if  $\kappa$  of nanoscale Si itself, the channel material of most microelectronic devices, can be drastically improved.

It had been hoped that isotope enrichment of semiconductors would raise  $\kappa$ , as mass disorder arising from isotopes (typically at a few percent or higher atomic fractions) are efficient scatterers to heat-carrying phonons [1,14–16]. The isotope effect of  $\kappa$  is described by the ratio  $P = (\kappa_{\text{iso}}/\kappa_{\text{nat}} - 1)$ , where  $\kappa_{\text{iso}}$  and  $\kappa_{\text{nat}}$  are the thermal conductivity of isotopically enriched material and the same material with natural isotope abundances, respectively. A high isotope factor  $P$  can arise from strong phonon scattering with isotopes, or conversely a weak umklapp scattering of phonons [1,15,16]. The former is favored by high isotope mass fluctuations [15]. The latter can be weak in the presence of acoustic phonon bunching combined with a wide band gap between acoustic and optical phonons [1,16]. Bulk silicon, unfortunately, meets none of these conditions, resulting in a weak isotope effect of  $P \approx 10\%$  at room temperature [17,18].

It has been reported that the isotope effect of  $\kappa$  becomes large in some low-dimensional materials. For example,  $\kappa$  was reported to be enhanced by  $\sim 50\%$  in isotopically enriched BN nanotubes at room temperature [19]. An even stronger isotope effect was recently discovered in cubic BN

crystals ( $P \sim 108\%$ ) [20]. A strong isotope effect in  $\kappa$  was also revealed in two dimensional materials, including graphene ( $\sim 50\%$ ) [21], monolayer MoS<sub>2</sub> ( $\sim 50\%$ ) [22], and monolayer BN ( $\sim 40\%$ ) [23,24]. For nanoscale Si, previous studies have reported that isotopically enriched <sup>29</sup>Si (99.9%) NWs grown by gold-catalyzed vapor phase epitaxy show  $\sim 30\%$  greater  $\kappa$  than <sup>28</sup>Si<sub>0.5</sub><sup>30</sup>Si<sub>0.5</sub> NWs, measured using Raman nanothermometry [25,26]. It is both intriguing and important to ask whether nanoscale Si prepared with top-down methods with naturally rough surfaces [9] would display a stronger isotope effect than bulk Si when isotope scattering, boundary scattering, and umklapp scattering of phonons all interplay and compete. The answer is not straightforward, as a first-order theory would expect the isotope scattering to be further overshadowed by the newly added boundary scattering, leading to  $P$  values even lower than in the bulk.

In this Letter, we prepared isotopically enriched <sup>28</sup>Si NWs as well as natural Si (<sup>nat</sup>Si) NWs with sub-100 nm diameters, and directly measured their thermal conductivity. We found that the isotope effect of  $\kappa$  is much enhanced from  $\sim 10\%$  in the bulk to 150% in the NWs. Using a model based on a combination of first-principles phonon dispersion and the phonon Boltzmann transport equation, we explain the effect with a two-way coupling between the two distinct phonon scattering mechanisms by mass disorder and by surface roughness. The rates of the two scattering mechanisms are mutually amplified in <sup>nat</sup>Si NWs, resulting in the unusually strong isotope effect in  $\kappa$  when the effect is eliminated in <sup>28</sup>Si NWs.

Si enriched in the isotope <sup>28</sup>Si in the form of SiF<sub>4</sub> was converted to bulk polycrystalline Si by a laboratory-scale reactor, and dislocation-free single crystals (Supplemental Material [27]) were produced from the polycrystalline Si by the float-zone technique [35]. The isotopic composition of the single crystals was measured using secondary ion mass spectroscopy (SIMS) to be 99.920% <sup>28</sup>Si, 0.075% <sup>29</sup>Si, and 0.005% <sup>30</sup>Si; this contrasts with the composition of <sup>nat</sup>Si: 92.23% <sup>28</sup>Si, 4.67% <sup>29</sup>Si, and 3.10% <sup>30</sup>Si. These <sup>28</sup>Si-enriched crystals (thereafter referred to as <sup>28</sup>Si) show a resistivity of approximately 10  $\Omega$  cm at room temperature with  $n$ -type conduction and free carrier concentration of  $3 \times 10^{14}$  cm<sup>-3</sup>, as reported in previous publications [35]. The concentration of impurities was determined by SIMS to be below  $10^{16}$  cm<sup>-3</sup> with carbon being the most prominent impurity. The <sup>28</sup>Si bulk crystal was then made into NWs using an electroless etching (EE) method in an aqueous solution of AgNO<sub>3</sub> and HF acid [5]. As a reference, <sup>nat</sup>Si NWs were also prepared using the same recipe from an  $n$ -type <sup>nat</sup>Si crystal with very similar resistivity ( $\sim 10$   $\Omega$  cm). The obtained Si NWs were individually dry transferred to a suspended pad microdevice using a sharp probe for measurement of thermal conductivity [55]. As shown in Fig. 1(a), such a microdevice consists of two suspended pads bridged by the NW to be

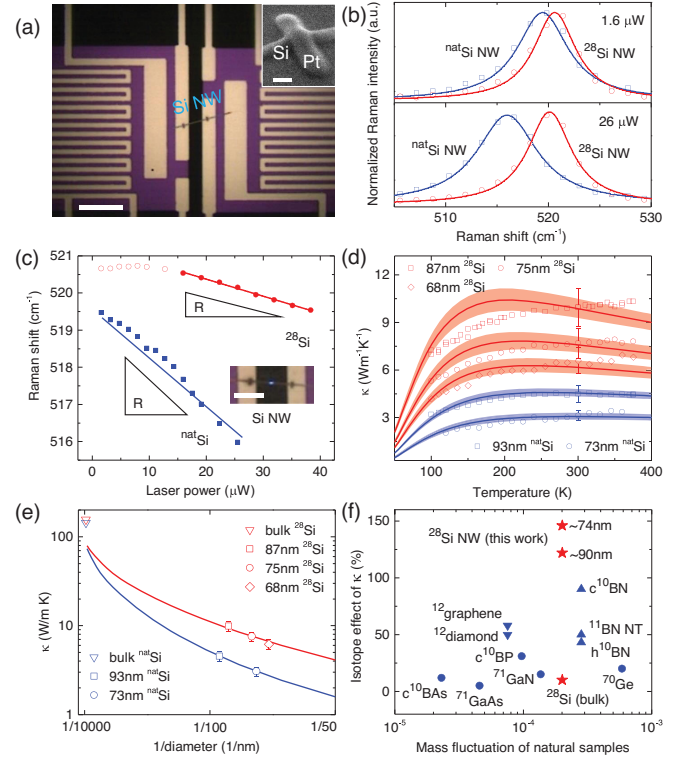


FIG. 1. Thermal conductivity of isotopically enriched (<sup>28</sup>Si at 99.92%) and natural Si NWs. (a) Optical image of a microdevice consisting of two suspended pads bridged by a Si NW. Inset: SEM image showing the Si NW FIB-bonded by Pt onto the underlying electrodes on the suspended pads. Scale bars: 10  $\mu$ m (main panel); 100 nm (Inset). (b) Normalized Raman spectra of suspended Si NWs at a low and a high laser power. (c) Raman peak position as a function of the laser power. Inset: optical image of a suspended NW, where the blue spot shows the focus of the laser beam. Scale bar: 5  $\mu$ m. (d) Temperature-dependent thermal conductivity of Si NWs. Symbols are experimental data; curves with shaded thickness are theoretical predictions with 3 nm roughness and  $6.5 \pm 0.1$  ( $5.1 \pm 0.1$ ) nm correlation length for the isotopically enriched (natural) Si NWs. (e) Calculated (curves) and measured (points) thermal conductivity of Si NWs as a function of reciprocal diameter at 300K. (f) Comparison of room-temperature isotope effect of  $\kappa$  of Si NWs compared with that of other isotopically enriched materials reported in the literature. Mass fluctuation parameter of elemental material ( $A$ ) and compound ( $AB$ ) is defined as  $g_A = \sum_i c_i (1 - M_i/M_{av})^2$  and  $g = [(g_A M_A^2 + g_B M_B^2)/(M_A + M_B)^2]$ , respectively, where  $c_i$  is the atomic fraction of the  $i$ th isotope.

measured [5,55,56]. Each pad has a Pt microheater and thermometer to control and sense the temperature, so thermal conductance of the NW can be measured by heat transported from the heating pad to the sensing pad [5,55].

Before accurately measuring the thermal conductivity, Raman spectra were taken from the Si NWs by focusing the laser at the middle of the suspended NWs [inset of Fig. 1(c)]. The Raman spectrum of <sup>28</sup>Si NW shows a blueshift with respect to that of <sup>nat</sup>Si NW with similar

diameter [Fig. 1(b)], which is expected from the lighter mean atomic mass of  $^{28}\text{Si}$  and consistent with results in bulk crystals (Supplemental Material [27]) [57,58]. When the laser power increases, the Raman peak of both NWs redshifts. This is expected as higher laser power heats more the suspended NW at the laser spot, resulting in a redshift of the NW's Raman peak. Interestingly, the  $^{\text{nat}}\text{Si}$  NW shows a much stronger redshift than the  $^{28}\text{Si}$  NW at the same, increased laser power, which suggests more heat accumulation at the laser spot [59], attributed to a much lower  $\kappa$  of the  $^{\text{nat}}\text{Si}$  NW. From the rates of the redshift, it can be estimated that  $\kappa$  of the  $^{28}\text{Si}$  NW is approximately two times higher than that of the  $^{\text{nat}}\text{Si}$  NW [see Fig. 1(c) and Supplemental Material [27]].

Using the heating and sensing micropads,  $\kappa$  of  $^{28}\text{Si}$  and  $^{\text{nat}}\text{Si}$  NWs with various diameters were directly measured over a range of temperatures, as shown in Fig. 1(d). The  $\kappa$  values of  $^{\text{nat}}\text{Si}$  NWs are in good agreement with what has been reported in literature for synthesis with the EE method [5].

More strikingly, an unusually high isotope effect is observed in these NWs. The Si NWs show an isotope effect ( $\kappa_{\text{iso}}/\kappa_{\text{nat}} - 1$ ) of  $\sim 120\%$  and  $\sim 150\%$  for NWs with diameter of  $\sim 90$  nm and  $\sim 74$  nm, respectively [Fig. 1(e)]. We also measured  $\kappa$  of bulk crystals of  $^{28}\text{Si}$  and  $^{\text{nat}}\text{Si}$  using time domain thermoreflectance (TDTR) and found  $\kappa_{\text{iso}}/\kappa_{\text{nat}} - 1$  to be only  $\sim 10\%$  (Supplemental Material [27]). This low isotope effect in bulk Si is consistent with previous studies [17,18], and is understandable because at room temperature isotope scattering of phonons in  $^{\text{nat}}\text{Si}$  would be overshadowed by the much stronger umklapp phonon scattering. The observed isotope effect of Si NWs is shown in Fig. 1(f) together with the values of isotope effect of other bulk and low-dimensional materials, including 5% for GaAs [60], 31% for BP [10], 12% for BAs [20], 20% for Ge [61], 15% for GaN [62], 50% for diamond [63], 50% for monolayer  $\text{MoS}_2$  [22], 50% for BN nanotube [19], and 108% for cubic BN [20]. The isotope enhancement of  $\kappa$  observed in  $^{28}\text{Si}$  NWs is exceedingly high compared to all other materials reported.

It is known that thermal conductivity of NWs is very sensitive to not only the diameter, but also the surface roughness profile of the NWs [5,6]. The roughness of an NW is typically characterized by two parameters: the root-mean-square value of the NW's surface height fluctuation ( $\Delta$ ), and the correlation length ( $L$ ) defined as the mean distance between roughness peaks, as illustrated in Fig. 2(a). According to the model by Martin *et al.* [6], which introduced roughness scattering rates derived from perturbation theory in Fermi's golden rule, a shorter correlation length drives the surface scattering of phonons toward a more diffusive process, leading to a suppression of  $\kappa$  below the so-called Casimir limit. The importance of correlation length in explaining thermal conductivity values below the Casimir limit in Si NWs was confirmed by

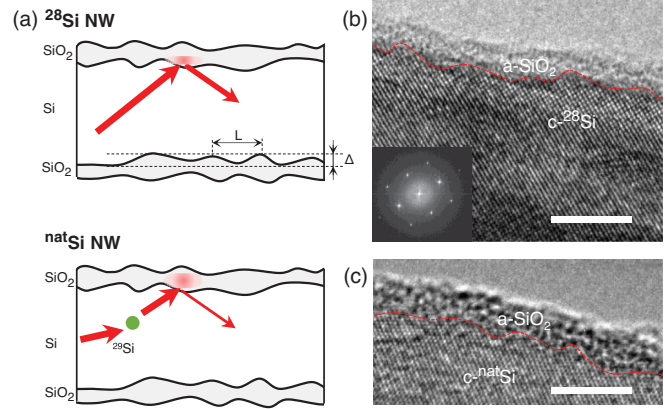


FIG. 2. Schematic of phonon scattering on the Si/SiO<sub>2</sub> interface and structural characterization of the Si NWs. (a) Schematic of phonon scattering on the *c*-Si core/*a*-SiO<sub>2</sub> shell interface of  $^{28}\text{Si}$  and  $^{\text{nat}}\text{Si}$  NWs, where  $\Delta$  and  $L$  indicate the roughness amplitude and physical correlation length, respectively. Phonon scattering back to the Si core occurs dominantly on the interface in  $^{28}\text{Si}$  NWs; in  $^{\text{nat}}\text{Si}$  NWs, in contrast, a higher portion of phonon wave packets transmits into the *a*-SiO<sub>2</sub> shell, effectively shortening the correlation length and significantly reducing the thermal conductivity of the NW. (b) and (c) high-resolution TEM images and fast Fourier transform (FFT, inset) of a  $^{28}\text{Si}$  NW and a  $^{\text{nat}}\text{Si}$  NW. Surface roughness, highlighted by the red dashed line, is evident on the interface between the crystalline Si core (*c*-Si) and the native amorphous SiO<sub>2</sub> shell (*a*-SiO<sub>2</sub>). Scale bar is 4 nm in both (b) and (c).

subsequent models based on nonequilibrium Green's functions [64], phonon Monte Carlo transport simulations [54], and experiments [7,65,66]. In our Letter, using high-resolution transmission electron microscopy (TEM), both  $^{\text{nat}}\text{Si}$  and  $^{28}\text{Si}$  NWs were determined to be single crystalline, as shown in Figs. 2(b) and 2(c). Indeed, unlike the smooth surface of Si NWs grown by the gold-catalyzed VPE method [25,26,67], these Si NWs have a rough surface with physical roughness on the order of several nanometers, surrounded by native, amorphous SiO<sub>2</sub> (*a*-SiO<sub>2</sub>) with a thickness of  $2 \sim 3$  nm. The rough morphology of these EE method synthesized Si NWs is consistent with what has been reported previously [5]. More importantly, the  $^{28}\text{Si}$  and  $^{\text{nat}}\text{Si}$  NWs do not have noticeable difference in the physical roughness and native SiO<sub>2</sub> thickness. This is not surprising because the  $^{28}\text{Si}$  and  $^{\text{nat}}\text{Si}$  NWs were both synthesized following the same EE recipe from two starting bulk materials that have the same doping type and nearly the same electrical conductivity. Their major difference, the different isotopic purities in the  $^{28}\text{Si}$  and  $^{\text{nat}}\text{Si}$  materials, is not expected to cause any difference in the EE process where the NWs and native SiO<sub>2</sub> form.

To elucidate the much stronger isotope effect than in the bulk, we employ a numerical model by solving the phonon Boltzmann transport equation with phonon dispersions determined from first principles. The total relaxation time

( $\tau_{\text{tot}}$ ) is composed of that attributed to normal phonon-phonon ( $N$ ), umklapp three-phonon ( $U$ ), boundary ( $B$ ), and isotope (iso) scatterings; that is,  $\tau_{\text{tot}}^{-1} = \tau_N^{-1} + \tau_U^{-1} + \tau_B^{-1} + \tau_{\text{iso}}^{-1}$  [14,68]. In conventional “decoupled” models, we consider all these four scattering processes to be independent, hence simply add the bulk isotope scattering rates to the NW boundary scattering rate. This “decoupled” treatment results in virtually no discernible difference in  $\kappa$  between  $^{28}\text{Si}$  and  $^{\text{nat}}\text{Si}$  NWs in our calculation, and therefore is not able to explain the experimental results. This is because, unlike bulk Si where isotope scattering contributes about 10% to  $\kappa$  at room temperature, there is a more than tenfold increase in phonon scattering from boundaries in Si NWs, significantly dwarfing the contribution from isotope scattering. Therefore, a coupling between phonon-isotope scattering and phonon-boundary scattering has to be taken into account.

We propose a two-way interaction between the scattering by isotope mass disorder and that by boundary roughness disorder, termed as the “coupled” model in this Letter. First, the surface roughness combined with small diameters of the NWs results in strong boundary scattering, making the lifetime of phonons so short that we need to consider collisional broadening. Phonon lines are broadened according to the uncertainty principle. We capture this by replacing the energy-conserving  $\delta$  function in the vibrational density of states (VDOS) by a homogeneously broadened Lorentzian distribution. The width of the distribution is related to the total scattering rate,  $\gamma_b(\vec{q}) = \hbar/2\tau_{b,\text{tot}}(\vec{q})$  [69,70], to obtain the vibrational spectrum  $D_b(\omega) = \int [d\vec{q}/(2\pi)^3] (1/\pi) \{ \gamma_b(\vec{q}) / [(\omega - \omega_b(\vec{q}))^2 + \gamma_b(\vec{q})^2] \}$ . Using this broadened spectrum in place of the VDOS results in the NW isotope scattering rates shown by red dots in Fig. 3(a). This “coupled” isotope scattering rate is significantly

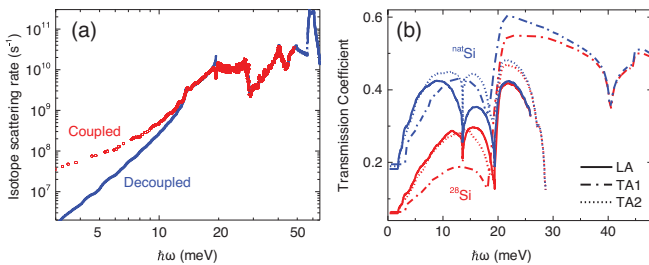


FIG. 3. Calculation of two-way coupled phonon dynamics involving surface roughness and isotope mass disorder in Si NWs. (a) Isotope scattering rates in a  $^{\text{nat}}\text{Si}$  NW (90 nm diameter) by the “decoupled” model compared to the “coupled” model. In the energy range below 20 meV, the isotope scattering is remarkably enhanced by the presence of the surface  $\text{SiO}_2$ . (b) Transmission coefficient spectrum of different phonon branches from  $c$ -Si to  $a$ - $\text{SiO}_2$  for  $^{28}\text{Si}$  vs  $^{\text{nat}}\text{Si}$ .  $^{\text{nat}}\text{Si}$  shows a higher transmission coefficient at low phonon energies, implying stronger roughness scattering at the Si/SiO<sub>2</sub> interface enhanced by isotopes.

higher than the “decoupled” one at the same isotope composition, especially for phonon energies below  $\sim 15$  meV. The coupling is also analogous to the drastic influence from vacancies on flexural phonons scattering in graphene [71]. However, even after this roughness-enhanced isotope scattering rate, it is still not sufficiently high to compete with the boundary scattering rate in NWs. Our calculations show that this “one-way coupling” between the two rates, where boundary roughness scattering enhances the isotope rate, in  $^{\text{nat}}\text{Si}$  NWs only results in a 5% decrease in  $\kappa$  relative to  $^{28}\text{Si}$  NWs with comparable diameter and roughness. Therefore, the opposite direction, the amplification of roughness scattering by the presence of isotopes, needs to be covered to constitute a “two-way coupled” model.

Indeed, it has been shown that across the SiC/GaN interface, interfacial phonon transfer is enhanced by the presence of 5% Ga isotopes, raising thermal boundary conductance by  $\sim 20\%$  [72]. In our NWs, the  $\text{SiO}_2$  shell is amorphous, where atoms completely lose long-range order and spatial correlation. Therefore, phonons transmitted into the  $a$ - $\text{SiO}_2$  shell encounter much stronger disorder scattering than if they are scattered back to the crystalline Si core at the Si/SiO<sub>2</sub> interface, as illustrated in Fig. 2(a). Physically, increasing the mass disorder with isotopes and the resultant stronger phonon scattering in the  $c$ -Si core leads to a better vibrational match with the  $a$ - $\text{SiO}_2$  shell, resulting in a higher transmission rate of phonon wave packets into the latter. As shown in Fig. 3(b), this is demonstrated by the higher phonon transmission coefficient across the  $^{\text{nat}}\text{Si}/\text{SiO}_2$  interface than the  $^{28}\text{Si}/\text{SiO}_2$  interface, as calculated by the full-band scattering-mediated diffuse mismatch model, obtained by combining the scattering-mediated acoustic mismatch model [31,43] with the full-band diffuse mismatch model (Supplemental Material, Note 2 [27]).

The higher phonon transmission coefficient in the  $^{\text{nat}}\text{Si}$  NW to its  $\text{SiO}_2$  shell gives rise to a shorter effective correlation length than in the  $^{28}\text{Si}$  NW, despite that they have comparable roughness and hence similar physical correlation length along the Si/SiO<sub>2</sub> boundary. This feedback from the isotope scattering back to the boundary scattering is captured in our calculation by reducing the effective correlation length in the surface scattering rate from  $6.5 \pm 0.1$  nm for the  $^{28}\text{Si}$  NWs to  $5.1 \pm 0.1$  nm for the  $^{\text{nat}}\text{Si}$  NWs. Surface scattering is proportional to the roughness power spectrum [6]  $S(k) = 2\pi\Delta^2L^2/(1 + L^2k^2)^{3/2}$ , which quantitatively relates the scattering rate to the roughness  $\Delta$  and the correlation length  $L$  [7], as described in Supplemental Material [27]. In addition, it constrains scattering to those in which the change in phonon wave vector,  $k = |\vec{q} - \vec{q}'|$ , is smaller than the inverse of the correlation length, as the power spectrum decays as  $1/k^3$  when  $kL \gg 1$  [45]. Consequently, roughness scattering is highly sensitive to the roughness power spectrum  $S(k)$  [7],

which is characterized by a combination of  $\Delta$  and  $L$ . A shorter  $L$  broadens the phase space for scattering [64], which increases the scattering rate and leads to lower thermal conductivity in  $^{nat}\text{Si}$  NW. Using this shortened  $L$ , an  $\sim 150\%$  isotope enhancement in  $\kappa$  was reproduced for  $^{28}\text{Si}$  NWs of diameter of 74 nm, in agreement with the experimental results, as shown in Figs. 1(d) and 1(e).

The correlation length for phonon scattering is equal to the physical correlation length at the Si/SiO<sub>2</sub> interface only if all phonons are scattered back to the  $c$ -Si core without transmission into the  $a$ -SiO<sub>2</sub>. In the other extreme, when phonons reaching the Si/SiO<sub>2</sub> interface all transmit into the  $a$ -SiO<sub>2</sub> shell, they would experience a total loss of long-range correlation. In between these two extrema, we loosely assume a linear interpolation and write the effective correlation length approximately as  $L = L_{\text{physical}}(1 - t)$ , where  $t$  represents the transmission coefficient of phonons at the Si/SiO<sub>2</sub> interface. Because the most significant portion of heat carriers are those phonons with energies below  $k_B T$ , we estimate from Fig. 3(b) the averaged transmission coefficient from  $^{28}\text{Si}$  and  $^{nat}\text{Si}$  to  $a$ -SiO<sub>2</sub> to be 0.2 and 0.4, respectively. This treatment leads to a ratio of  $L$  equal to approximately 1.3 between the cases of  $^{28}\text{Si}$  and  $^{nat}\text{Si}$  NWs, consistent with the values of  $L = 6.5$  nm for  $^{28}\text{Si}$  and 5.1 nm for  $^{nat}\text{Si}$  that were used in the simulations to reach good agreement with the experimental data in Fig. 1(e). We note that a similar considerable effect of the presence of amorphous shell around ultrathin Si nanowires was found in nonequilibrium Greens' function [73] and molecular dynamics simulations [74].

In conclusion, we discovered that the thermal conductivity of isotopically enriched  $^{28}\text{Si}$  NWs shows an unusual contrast, up to 2.5 times higher at room temperature, than that of  $^{nat}\text{Si}$  NWs with similar diameters and surface morphology. This is in stark contrast to the behavior of bulk Si, where the isotopically enriched one is only 10% higher. Our Boltzmann transport model with first-principles phonon dispersion explains this giant isotope effect as a two-way coupling of boundary scattering and isotope scattering, correlated via transmission of phonons to the native amorphous SiO<sub>2</sub> shell in NWs. Our results reveal a mutual enhancement of two distinct scattering mechanisms and offer deep insights to heat transfer crossing or in presence of crystalline-amorphous interfaces. It also inspires potential applications of isotopically engineered semiconductors in the pursuit of efficient thermal management in Si-based modern microelectronics. From a broad perspective,  $^{28}\text{Si}$  is appealing for high-fidelity quantum computation due to the absence of nuclear spin [75–77]. It is also important to show and understand the distinctly different phonon behavior in nanoscale  $^{28}\text{Si}$  from the perspective of enhancing coherence in quantum systems.

This work was funded by the U.S. Department of Energy, Office of Science, Office of Basic Energy

Sciences, Materials Sciences and Engineering Division under Contract No. DE-AC02-05-CH11231 (EMAT program KC1201) (Materials processing, device fabrication, measurements, data analysis, and simulation). The thermal characterization of devices used facilities supported by U.S. NSF Grant No. ECCS-1953803. Z. A. acknowledges support from U.S. National Science Foundation (Grant No. 1902352). M. R. J. would like to acknowledge the David and Lucile Packard Foundation (Grant No. 2018-68049) for financial support. H. S. and B. S. acknowledge the support from NSFC No. 12004211 and Shenzhen Science and Technology Program No. RCYX202007141-14643187. We thank Professor Eric Pop for helpful discussions.

J. W. and P. C. conceived the project. J. A. synthesized and characterized the bulk  $^{28}\text{Si}$  crystals. P. C. produced the Si NWs from bulk Si crystals, fabricated the devices, and performed Raman and thermal measurement via suspended pads microdevices, with the help of L. J. M. S and M. R. J. contributed to TEM characterization. H. S. and B. S. measured the thermal conductivity of bulk Si by TDTR. Z. A. developed the numerical model and M. U. performed the calculations. All authors discussed and contributed to the preparation of the manuscript.

\*To whom correspondence should be addressed.  
zlatan.aksamija@utah.edu

Present address: Department of Materials Science and Engineering, University of Utah, Salt Lake City, Utah 84112, USA.

†To whom correspondence should be addressed.  
wuj@berkeley.edu

- [1] L. Lindsay, D. A. Broido, and T. L. Reinecke, *Phys. Rev. Lett.* **111**, 025901 (2013).
- [2] S. Ghosh, I. Calizo, D. Teweldebrhan, E. P. Pokatilov, D. L. Nika, A. A. Balandin, W. Bao, F. Miao, and C. N. Lau, *Appl. Phys. Lett.* **92**, 151911 (2008).
- [3] R. Chen, A. I. Hochbaum, P. Murphy, J. Moore, P. D. Yang, and A. Majumdar, *Phys. Rev. Lett.* **101**, 105501 (2008).
- [4] D. Y. Li, Y. Y. Wu, P. Kim, L. Shi, P. D. Yang, and A. Majumdar, *Appl. Phys. Lett.* **83**, 2934 (2003).
- [5] A. I. Hochbaum, R. K. Chen, R. D. Delgado, W. J. Liang, E. C. Garnett, M. Najarian, A. Majumdar, and P. D. Yang, *Nature (London)* **451**, 163 (2008).
- [6] P. Martin, Z. Aksamija, E. Pop, and U. Ravaioli, *Phys. Rev. Lett.* **102**, 125503 (2009).
- [7] J. W. Lim, K. Hippalgaonkar, S. C. Andrews, A. Majumdar, and P. D. Yang, *Nano Lett.* **12**, 2475 (2012).
- [8] B. Yu *et al.*, in *International Electron Devices Meeting, San Francisco, Technical Digest* (IEEE, New York, 2002), pp. 251–254, [10.1109/IEDM.2002.1175825](https://doi.org/10.1109/IEDM.2002.1175825).
- [9] N. Singh, A. Agarwal, L. K. Bera, T. Y. Liow, R. Yang, S. C. Rustagi, C. H. Tung, R. Kumar, G. Q. Lo, N. Balasubramanian, and D.-L. Kwong, *IEEE Electron Device Lett.* **27**, 383 (2006).

- [10] Q. Y. Zheng, S. Li, C. H. Li, Y. C. Lv, X. Y. Liu, P. Y. Huang, D. A. Broido, B. Lv, and D. G. Cahill, *Adv. Funct. Mater.* **28**, 1805116 (2018).
- [11] F. Tian *et al.*, *Science* **361**, 582 (2018).
- [12] J. S. Kang, M. Li, H. A. Wu, H. Nguyen, and Y. J. Hu, *Science* **361**, 575 (2018).
- [13] S. Li, Q. Y. Zheng, Y. C. Lv, X. Y. Liu, X. Q. Wang, P. Huang, D. G. Cahill, and B. Lv, *Science* **361**, 579 (2018).
- [14] D. T. Morelli, J. P. Heremans, and G. A. Slack, *Phys. Rev. B* **66**, 195304 (2002).
- [15] L. Lindsay, D. A. Broido, and T. L. Reinecke, *Phys. Rev. B* **88**, 144306 (2013).
- [16] L. Lindsay, D. A. Broido, and T. L. Reinecke, *Phys. Rev. Lett.* **109**, 095901 (2012).
- [17] A. V. Inyushkin, A. N. Taldenkov, A. M. Gibin, A. V. Gusev, and H. J. Pohl, *Phys. Status Solidi C* **1**, 2995 (2004).
- [18] T. Ruf, R. W. Henn, M. Asen-Palmer, E. Gmelin, M. Cardona, H. J. Pohl, G. G. Devyatych, and P. G. Sennikov, *Solid State Commun.* **115**, 243 (2000).
- [19] C. W. Chang, A. M. Fennimore, A. Afanasiev, D. Okawa, T. Ikuno, H. Garcia, D. Y. Li, A. Majumdar, and A. Zettl, *Phys. Rev. Lett.* **97**, 085901 (2006).
- [20] K. Chen *et al.*, *Science* **367**, 555 (2020).
- [21] S. S. Chen, Q. Z. Wu, C. Mishra, J. Y. Kang, H. J. Zhang, K. J. Cho, W. W. Cai, A. A. Balandin, and R. S. Ruoff, *Nat. Mater.* **11**, 203 (2012).
- [22] X. F. Li *et al.*, *ACS Nano* **13**, 2481 (2019).
- [23] Q. R. Cai, D. Scullion, W. Gan, A. Falin, P. Cizek, S. Liu, J. H. Edgar, R. Liu, B. C. C. Cowie, E. J. G. Santos, and L. H. Li, *Phys. Rev. Lett.* **125**, 085902 (2020).
- [24] L. Lindsay and D. A. Broido, *Phys. Rev. B* **84**, 155421 (2011).
- [25] S. Mukherjee *et al.*, *Nano Lett.* **15**, 3885 (2015).
- [26] S. Mukherjee, U. Givan, S. Senz, M. de la Mata, J. Arbiol, and O. Moutanabbir, *Nano Lett.* **18**, 3066 (2018).
- [27] See Supplemental Material at <http://link.aps.org/supplemental/10.1103/PhysRevLett.128.085901> for experimental methods and theoretical calculations, which includes Refs. [28–54].
- [28] G. Gilat and L. J. Raubenheimer, *Phys. Rev.* **144**, 390 (1966).
- [29] P. Giannozzi *et al.*, *J. Phys. Condens. Matter* **29**, 465901 (2017).
- [30] Z. Aksamija and I. Knezevic, *Phys. Rev. B* **82**, 045319 (2010).
- [31] P. Reddy, K. Castelino, and A. Majumdar, *Appl. Phys. Lett.* **87**, 211908 (2005).
- [32] J. M. Ziman, *Electrons and Phonons* (Oxford University Press, London, 1960).
- [33] M. Upadhyaya, S. N. Khatami, and Z. Aksamija, *J. Mater. Res.* **30**, 2649 (2015).
- [34] K. Esfarjani, G. Chen, and H. T. Stokes, *Phys. Rev. B* **84**, 085204 (2011).
- [35] J. W. Ager, J. W. Beeman, W. L. Hansen, E. E. Haller, I. D. Sharp, C. Liao, A. Yang, M. L. W. Thewalt, and H. Riemann, *J. Electrochem. Soc.* **152**, G448 (2005).
- [36] P. B. Allen, *Phys. Rev. B* **88**, 144302 (2013).
- [37] A. Ward and D. A. Broido, *Phys. Rev. B* **81**, 085205 (2010).
- [38] J. A. Pascual-Gutierrez, J. Y. Murthy, and R. Viskanta, *J. Appl. Phys.* **102**, 034315 (2007).
- [39] D. G. Cahill, S. K. Watson, and R. O. Pohl, *Phys. Rev. B* **46**, 6131 (1992).
- [40] C. Wang, Y. Tamai, and N. Kuzuu, *J. Non-Cryst. Solids* **321**, 204 (2003).
- [41] M. Upadhyaya and Z. Aksamija, *Phys. Rev. B* **94**, 174303 (2016).
- [42] P. Giannozzi *et al.*, *J. Phys. Condens. Matter* **21**, 395502 (2009).
- [43] R. S. Prasher and P. E. Phelan, *J. Heat Transf. Trans. ASME* **123**, 1194 (2001).
- [44] G. S. Doerk, C. Carraro, and R. Maboudian, *ACS Nano* **4**, 4908 (2010).
- [45] D. Gelda, M. G. Ghossoub, K. Valavala, J. Ma, M. C. Rajagopal, and S. Sinha, *Phys. Rev. B* **97**, 045429 (2018).
- [46] S. B. Soffer, *J. Appl. Phys.* **38**, 1710 (1967).
- [47] K. F. Murphy, B. Piccione, M. B. Zanjani, J. R. Lukes, and D. S. Gianola, *Nano Lett.* **14**, 3785 (2014).
- [48] C. J. Foss and Z. Aksamija, *J. Appl. Phys.* **120**, 225104 (2016).
- [49] J. Carrete, L. J. Gallego, L. M. Varela, and N. Mingo, *Phys. Rev. B* **84**, 075403 (2011).
- [50] P. Carruthers, *Rev. Mod. Phys.* **33**, 92 (1961).
- [51] P. G. Klemens, *Solid State Phys.* **7**, 1 (1958).
- [52] G. A. Slack, *Solid State Phys.* **34**, 1 (1979).
- [53] Z. Aksamija and I. Knezevic, *Phys. Rev. B* **88**, 155318 (2013).
- [54] L. N. Maurer, Z. Aksamija, E. B. Ramayya, A. H. Davoody, and I. Knezevic, *Appl. Phys. Lett.* **106**, 133108 (2015).
- [55] S. Lee *et al.*, *Nat. Commun.* **6**, 8573 (2015).
- [56] P. Kim, L. Shi, A. Majumdar, and P. L. McEuen, *Phys. Rev. Lett.* **87**, 215502 (2001).
- [57] F. Widulle, T. Ruf, M. Konuma, I. Silier, M. Cardona, W. Kriegseis, and V. I. Ozhogin, *Solid State Commun.* **118**, 1 (2001).
- [58] P. V. Enkovich, V. V. Brazhkin, S. G. Lyapin, A. P. Novikov, A. V. Gusev, V. A. Gavva, M. F. Churbanov, and S. M. Stishov, *J. Phys. Commun.* **1**, 055005 (2017).
- [59] G. S. Doerk, C. Carraro, and R. Maboudian, *Phys. Rev. B* **80**, 073306 (2009).
- [60] V. Inyushkin, A. N. Taldenkov, A. Y. Yakubovskiy, A. V. Markov, L. Moreno-Garsia, and B. N. Sharonov, *Semicond. Sci. Technol.* **18**, 685 (2003).
- [61] M. AsenPalmer, K. Bartkowski, E. Gmelin, M. Cardona, A. P. Zhernov, A. V. Inyushkin, A. Taldenkov, V. I. Ozhogin, K. M. Itoh, and E. E. Haller, *Phys. Rev. B* **56**, 9431 (1997).
- [62] Q. Y. Zheng, C. H. Li, A. Rai, J. H. Leach, D. A. Broido, and D. G. Cahill, *Phys. Rev. Mater.* **3**, 014601 (2019).
- [63] T. R. Anthony, W. F. Banholzer, J. F. Fleischer, L. H. Wei, P. K. Kuo, R. L. Thomas, and R. W. Pryor, *Phys. Rev. B* **42**, 1104 (1990).
- [64] J. Sadhu and S. Sinha, *Phys. Rev. B* **84**, 115450 (2011).
- [65] K. Hippalgaonkar, B. Huang, R. Chen, K. Sawyer, P. Ercius, and A. Majumdar, *Nano Lett.* **10**, 4341 (2010).
- [66] M. G. Ghossoub, K. V. Valavala, M. Seong, B. Azeredo, K. Hsu, J. S. Sadhu, P. K. Singh, and S. Sinha, *Nano Lett.* **13**, 1564 (2013).
- [67] O. Moutanabbir, S. Senz, Z. Zhang, and U. Gosele, *Nano Today* **4**, 393 (2009).
- [68] J. Callaway, *Phys. Rev.* **113**, 1046 (1959).
- [69] S. I. Tamura, *Phys. Rev. B* **27**, 858 (1983).

- [70] J. Menendez and M. Cardona, *Phys. Rev. B* **29**, 2051 (1984).
- [71] G. Bouzerar, S. Thebaud, S. Pecorario, and C. Adessi, *J. Phys. Condens. Matter* **32**, 295702 (2020).
- [72] E. Lee and T.F. Luo, *Appl. Phys. Lett.* **112**, 011603 (2018).
- [73] N. Mingo and L. Yang, *Phys. Rev. B* **68**, 245406 (2003).
- [74] D. Donadio and G. Galli, *Phys. Rev. Lett.* **102**, 195901 (2009).
- [75] J. J. L. Morton, A. M. Tyryshkin, R. M. Brown, S. Shankar, B. W. Lovett, A. Ardavan, T. Schenkel, E. E. Haller, J. W. Ager, and S. A. Lyon, *Nature (London)* **455**, 1085 (2008).
- [76] S. Simmons, R. M. Brown, H. Riemann, N. V. Abrosimov, P. Becker, H. J. Pohl, M. L. W. Thewalt, K. M. Itoh, and J. J. L. Morton, *Nature (London)* **470**, 69 (2011).
- [77] A. M. Tyryshkin, S. Tojo, J. J. L. Morton, H. Riemann, N. V. Abrosimov, P. Becker, H.-J. Pohl, T. Schenkel, M. L. W. Thewalt, K. M. Itoh, and S. A. Lyon, *Nat. Mater.* **11**, 143 (2012).